LRP 490/94   January 1994

ROLE OF METASTABLE ATOMS IN ARGON-DILUTED SILANE RF PLASMAS

L. Sansonnens, A.A. Howling, Ch. Hollenstein,
J.L. Dorier & U. Kroll

ROLE OF METASTABLE ATOMS IN ARGON-DILUTED SILANE RF PLASMAS

L Sansonnens, A A Howling, Ch Hollenstein, J-L Dorier and U Kroll*

Centre de Recherches en Physique des Plasmas

Ecole Polytechnique Fédérale de Lausanne

21 Av. des bains, CH-1007 Lausanne, Switzerland

* Institut de Microtechnique, Université de Neuchâtel

Rue Bréguet 2, CH-2000 Neuchâtel - Switzerland

Abstract. The evolution of the argon metastable density has been studied by absorption spectroscopy in power-modulated plasmas of argon and a mixture of 4% silane in argon. A small concentration of silane suppresses the argon metastable density by molecular quenching. This molecular quenching adds to the electronic collisional dissociation to increase the silane dissociation rate as compared with pure silane plasmas. Using time-resolved emission spectroscopy, the role of metastables in excitation to the argon $2P_2$ state has been determined in comparison with production from the ground state. In silane plasmas, emission from SiH^* is due essentially to electron impact dissociation of silane, whereas in 4% silane-in-argon plasmas, emission from SiH^* seems to be due to electron impact excitation of the SiH ground state. These studies demonstrate that argon is not simply a buffer gas but has an influence on the dissociation rate in the plasma-assisted deposition of amorphous silicon using argon-diluted silane plasmas.

1. Introduction

The plasma-assisted deposition of amorphous hydrogenated silicon (a-Si:H) is used for the industrial production of solar cells and other electronic devices based on silicon. Since the understanding of the deposition process is mostly empirical, there remains a large scope for potential improvements. Numerous studies report on the influence on the film of silane dilution with noble gases [1-4] or with hydrogen [5]. Knight et al [3] have shown that dilution of silane with noble gases results in a small increase in the deposition rate, but also increases defect concentrations and can result in films with columnar structure. Matsuda et al [4] have reported that a-Si:H films deposited with xenon dilution of silane show less light-induced degradation and a greater degree of inhomogeneity in the network structure. Generally, these studies are made in term of film properties and the role of the noble gas in determining the plasma properties is less well known. Hollenstein et al [2] have shown that the degree of ionisation of silane radicals increases strongly and the ionic composition changes with noble gas dilution.

The consequences of diluting reactive gases with noble gases is not well understood. Ground state atoms of noble gases are inert and so any changes in discharge chemistry must result indirectly from changes in the electron, ion and neutral species. Metastable states of noble gases have often been studied [6-12] because they are supposed to play an important role in neutral reactions with chemically-reactive molecules [10,12]. The importance of metastable chemistry, relative to electronic and ionic chemistry, in altering the overall discharge chemistry is still unclear. One might

expect that metastable energy transfer would lead directly to increased dissociation and thereby influence plasma deposition processes.

In this work, we use on/off rf power modulation at 1 kHz to study the formation and destruction of different species. R f modulation might have application in this type of plasmas since it is know that modulation reduces powder formation [13,14], but in addition it also allows information on excited states [15-17]. Time-resolved optical emission and absorption spectroscopy are used because these are non-perturbing diagnostics which permit the simultaneous study of several excited species. We present the results of a study into the role of argon metastable states in plasma deposition when silane is diluted with argon. The Ar (1s5) metastable density evolution is measured during a power modulation period using optical absorption spectroscopy for pure argon and for a 4% silane-in-argon plasma. These measurements show the quenching of the metastables by the silane gas. The evolution of the argon and the SiH emission during a period of modulation is also measured for the case of pure argon, pure silane and 4% silane-in-argon plasmas. This study shows the different excitation mechanisms in these three different plasmas.

2. Experimental arrangement

The reactor (Fig. 1) consists of two cylindrical electrodes, 13 cm diameter, 2.8 cm apart in a cubic vacuum vessel of side 40 cm. The reactor is heated to 100 °C and the gas enters through the side wall. The flowrates used are 30 sccm for silane plasmas, 50 sccm for argon plasmas, and a mixture of 48:2 sccm for argon-

silane in the diluted plasma experiments. The pressure was maintained at 0.1 Torr.

The upper electrode and reactor walls are grounded. The lower electrode has a grounded guard screen and is capacitively-coupled to a rf amplifier (10 kHz-200 MHz) via a matching circuit and directional power meter. The on/off power modulation is produced by mixing a 1 kHz square-wave signal into the 30 MHz rf generator signal by means of a Hewlett Packard 10534A mixer. The peak-to-peak voltage (V_{pp}) is measured with a passive probe mounted on the underside of the rf electrode, connected to a floating oscilloscope. V_{pp} is adjusted according to the gas mixture (92 V for argon and argon-diluted plasmas, 120 V for silane plasmas) so as to maintain a 4 W average power dissipation in the plasma, equivalent to 8 W effective power during the "on" period of the modulation [18]. The rise- and fall-time of the rf power is 0.2 μs.

The quartz observation windows are mounted on tubes 35 cm from the plasma thereby avoiding any deposition which would otherwise modify the measured intensities. The global light emission is collected by an optical fibre. A spectrometer and optical multichannel analyser (OMA) are used for spectroscopic analysis from 300 to 750 nm with 0.5 nm resolution. Time-resolution is achieved by gating the OMA (model EG&G 1455) with a pulse amplifier (EG&G 1304); a Tektronix pulse former is employed to generate variable delay gate pulses (width 3 μs) synchronised to the power modulation.

For the absorption spectroscopy, the external source was an argon spectral lamp (Philips model 93100), arranged to give a collimated beam between the electrodes. The transmitted intensity

was corrected for the plasma emission by subtracting the signal obtained with the lamp switched off. All intensity measurements are relative intensities uncorrected for the spectral sensitivity of the detection system.

3. Results and discussion

3.1 Argon metastable density in Argon and Argon/Silane Plasmas

The argon metastable density was measured by absorption spectroscopy. In this technique, the absorption of light by metastables in the plasma is measured for a reference source having a wavelength corresponding to an electronic transition between a metastable state and an excited state of argon. Fig. 2 shows part of the schematic energy level and transition diagram of the argon atom. The $1s_3$ and $1s_5$ are the metastable states and the $1s_2$ and $1s_4$ are the resonant states of argon. For the measurement of the $1s_5$ population, the transition between the $2p_2$ and $1s_5$ level is used. The wavelength (λ) of this transition is 696.54 nm. The density of metastables is calculated from the measured absorption as described by Jolly and Touzeau in reference [19]. Fig. 3 shows the temporal variation during a modulation period of the metastable atom density (level $1s_5$) for an argon plasma and a 4% silane-in-argon plasma. Only the $1s_5$ density is measured, but Ferreira et al [8] show that the $1s_3$ density is about 10 times lower in similar conditions.

For the case of argon, the average metastable density measured is approximately 10^{11} cm^{-3}. The density increases slightly when the rf power is switched on and decreases slightly

when the power is switched off during each modulation cycle. The metastable density can be described by the continuity equation [10]:

$$\frac{\partial n_m}{\partial t} = F_m(t) - L_m(t) - G_m(t) \tag{1}$$

where n_m is the density of argon metastables (cm^{-3}), $F_m(t)$ is the production rate (cm^{-3} s^{-1}), $L_m(t)$ is the collision loss rate (cm^{-3} s^{-1}) and $G_m(t)$ is the diffusion loss rate (cm^{-3} s^{-1}).

Metastable formation is principally by electron impact on ground state argon atoms. Such a reaction can only occur for the high-energy electron component of the plasma (threshold energy 11.55 eV), and therefore only when the rf power is on.

The diffusion is principally along the electrode axis, and can be expressed as [11]:

$$G_m(t) \approx \frac{D_m n_m}{\Lambda^2 p} = k_D \, n_m \tag{2}$$

where D_m (= 61 cm^2.s^{-1}.Torr [11]) is the metastable diffusion coefficient, $\Lambda \approx d/\pi$ (= 0.9 cm) is the characteristic length for fundamental mode diffusion (d = 2.8 cm is the interelectrode distance) and p (0.1 Torr in this case) is the pressure, from which $k_D = 767$ s^{-1} is the effective diffusive metastable loss rate.

In our conditions, the principal collision loss rate is due to electron collisions which require small energy exchanges between electrons and the metastables Ar$_m$ in order to produce a resonant state Ar$_r$ (see Fig. 2) which can subsequently relax by photon emission, according to the reaction [10]:
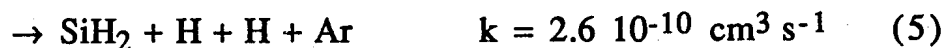
$$\text{Ar}_m \xrightarrow{\text{e}^-} \text{Ar}_r \rightarrow \text{Ar} + \text{h}\nu \qquad \text{with } L_m = k_e n_e n_m \qquad (3)$$

where n_e is the electron density and k_e (= $1.7 \cdot 10^{-7}$ cm^3 s^{-1} [11]) is the excitation rate of the metastable state ($1s_5$) to a resonant state. The dependence of k_e on electron temperature is not well known, but since the reaction energy threshold is very low (0.07 eV), we can assume that k_e does not vary strongly with the electron temperature T_e [10].

The relative importance of these two loss mechanisms can be estimated for the following plasma parameters: n_{Ar} (density of argon) = $3.4 \cdot 10^{15}$ cm^{-3}, n_m = 10^{11} cm^{-3} and n_e (electron density) = $2 \cdot 10^9$ cm^{-3} (corresponding to the value measured by Overzet and Hopkins [20] in similar plasma conditions). The electronic collision loss rate is then L_m = $3.3 \cdot 10^{13}$ cm^{-3} s^{-1} and the diffusion loss rate is G_m = $7.7 \cdot 10^{13}$ cm^{-3} s^{-1}. The value calculated for L_m is valid for the power on period; in the power off period, this value decreases as n_e decreases. The total loss rate estimated from Fig. 3 during the "power off" half-cycle (where metastable production is negligible) is approximately $8 \cdot 10^{13}$ cm^{-3} s^{-1}, which is in good agreement with the diffusion loss rate calculated above.

To a first approximation, the metastable production rate $F_m(t)$ can be estimated by supposing that the diffusion losses are constant during the whole modulation period and that the production and the electronic collision losses of metastables are constant during the "power on" half-cycle and zero during the "power off" half cycle. Such approximations yield a production rate $F_m(t)$ of about $2 \cdot 10^{14}$ cm^{-3} s^{-1} during the "power on" period. This value corresponds, for a plasma with n_e = $2 \cdot 10^9$ cm^{-3} and for the electronic excitation cross

section given by Theuws [21], to an electron temperature T_e of 2.6 eV, which is a reasonable value for these plasma conditions [22].

For the 4% silane-in-argon plasma, the measured metastable density (less than 10^{10} cm^{-3}) is very much smaller than for a pure argon plasma. Our measurement of the argon emission intensity (line 696·54 nm, transition $2p_2$-$1s_5$) as a function of the silane concentration in argon-silane plasmas shows that, below 10% silane concentration, this emitted intensity is at least as strong as for the case of the pure argon plasma. Since the excitation from the ground state to the $2p_2$ state and to the metastable states both depend on the hot electron component (threshold above 11.5 eV), we can therefore assume that the rate of production of metastables is not reduced when less than 10% silane is added to an argon plasma. The strong fall in metastable density in Fig. 3 for a 4% silane-in-argon plasma can therefore only be explained by introducing a supplementary loss mechanism due to metastable quenching by silane molecules and silane radicals. This quenching can dissociate these molecules: amongst the energetically possible reactions we can list, principally, the following examples [23]:

$$Ar_m + SiH_4 \rightarrow SiH_3 + H + Ar \qquad k = 1.4 \; 10^{-10} \; cm^3 \; s^{-1} \qquad (4)$$

$$\rightarrow SiH_2 + H + H + Ar \qquad k = 2.6 \; 10^{-10} \; cm^3 \; s^{-1} \qquad (5)$$

$$Ar_m + SiH_3 \rightarrow SiH_2 + H + Ar \qquad k = 1 \; 10^{-10} \; cm^3 \; s^{-1} \qquad (6)$$

$$Ar_m + SiH_2 \rightarrow SiH + H + Ar \qquad k = 1 \; 10^{-10} \; cm^3 \; s^{-1} \qquad (7)$$

$$Ar_m + SiH \rightarrow Si + H + Ar \qquad k = 1 \; 10^{-10} \; cm^3 \; s^{-1} \qquad (8)$$

For the plasma with 4% silane, these metastable quenching reactions become the dominant metastable loss mechanism and then their loss rate is equal to the production rate of metastables
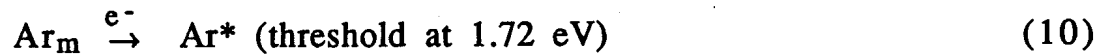
estimated for the pure argon plasma. For the reactions (4) and (5) and for a silane density of $1.2 \ 10^{14} \ cm^{-3}$, the metastable density required to obtain this loss rate must be equal to $3.9 \ 10^9 \ cm^{-3}$, which is correct to within the experimental error margin of the measurement in Fig. 3.

Comparison of the rate of these dissociative reactions in our dilution conditions with the rate of electron impact dissociation of the silane given by Kushner [23] in a pure silane plasma shows that these two rates are of the same order. Then, in the case of strong dilution of silane with argon, the argon not only plays the role of a buffer gas, but also take an active part via the quenching of the metastables on silane molecules, which adds to electron impact dissociation to increase the silane dissociation rate. Such behaviour has in fact been observed by Robertson and Gallagher [24] using mass spectrometry of radicals, as well as by Matras et al [25] by means of laser-induced fluorescence measurements of SiH concentration.

3.2 Emission from a modulated argon plasma

Fig. 4(a) shows the time variation of argon plasma emission at 696.54 nm (transition $2p_2$-$1s_5$) during one modulation cycle for an argon plasma. Three distinct periods can be distinguished: a transient period during the first 50 μs of the cycle, a stationary period for the remainder of the "power on" half-cycle, and finally the afterglow during the "power off" half-cycle. Fig. 4(b) shows in detail the decay of the Ar emission intensity for the initial 70 μs of the afterglow. The logarithmic plot shows a decay represented by two 1/e times. Similar results are also obtained by Cicala et al [15].

The observed time dependence in the three periods mentioned can be explained by analysing the excitation and emission mechanisms in the argon plasma. The non-metastable excited state $2p_2$ of argon (Ar*) can be obtained by electron impact on a ground state argon atom (equation 9), or by electron collision with an existing argon metastable (equation 10):

$$Ar \xrightarrow{e^-} Ar* \text{ (threshold at 13.27 eV)} \tag{9}$$

$$Ar_m \xrightarrow{e^-} Ar* \text{ (threshold at 1.72 eV)} \tag{10}$$

Collisional de-excitation is negligible compared to radiative decay at our low pressure. Since the lifetime of the excited state (26.5 ns [26]) is much shorter than the temporal variations in the emission shown in Fig. 4, the intensity emitted is proportional at all times to the total excitation rate and is given by:

$$I_{Ar*} \propto k_G \, n_e \, n_{Ar} + k_M \, n_e \, n_m \,, \tag{11}$$

where k_G and k_M are the rates of excitation from ground state and from metastable states respectively. They depend on the electron distribution function and reaction cross-sections.

To interpret the intensity variations in Fig. 4 it is necessary to determine the relative importance of the two excitation mechanisms throughout the modulation cycle. The different threshold energies for reactions (9) and (10) imply that variations in electron temperature T_e will more strongly influence the ground state excitation process. In Fig. 5 is shown the ratio of the production rates of the $2p_2$ excited state from the ground and from

metastable states as a function of T_e (assuming a Maxwellian distribution for the electrons) for a 0.1 Torr argon plasma with a 10^{11} cm^{-3} metastable density (as measured in Fig. 3). The production rates are taken from Theuws [21]. For $T_e < 2$ eV, it can be seen that excitation from the metastable states is dominant, whereas for $T_e > 3$ eV, excitation from the ground state dominates.

The peak in the transient period of Fig. 4(a) can be explained by an initial high temperature electron population [27] which reduces to its steady-state value as the electron density reaches equilibrium after 50 µs.

In the afterglow, the abrupt fall in intensity corresponds to a rapid decrease of T_e. The decrease of n_e, limited by ambipolar diffusion, is too slow to explain such a fast intensity decay. The two distinct decay times can be explained by the fact that the mechanisms for excited state production change as T_e decreases. In the initial rapid fall region in Fig. 4(b), the principal source of emission is by excitation from the ground state which decreases rapidly when T_e falls. In the second region, the emission comes from the excitation of the metastable states which depends on the lower energy electrons and then decreases slowly as T_e decreases. The persistence of cold electrons after more than 70 µs into the afterglow is compatible with other experiments [28] and is explained by ambipolar diffusion which constrains the electrons to diffuse at the same speed as the heavy positive ions.

If the second slope in Fig. 4(b) is extrapolated back to the beginning of the afterglow, the relative contribution of the ground state and the metastable states to the production of the excited sates can be estimated. We thereby estimate that the excitation rate

from the ground state is twice as large as the corresponding rate originating from the metastable state during the steady-state period. From Fig. 5, this situation corresponds to a steady-state electron temperature of 2.6 eV which is the same as the estimation obtained with the metastable production rate in section 3.1.

3.3 Emission from a modulated silane plasma

Fig. 6(a) presents the SiH* emission at 414.23 nm (transition $A^2\Delta$ - $X^2\Pi$) during a modulation cycle for a pure silane plasma. As for argon, three distinct periods are observed. Fig. 6(b) shows that, in this case, the intensity decays with a single 1/e time of 5 µs in the afterglow.

These results can be interpreted by consideration of the dominant excitation mechanism for SiH* starting from SiH_4. In pure silane the SiH* is produced by electron dissociation of the SiH_4 [15,29,30]:

$$SiH_4 \xrightarrow{e^-} SiH_4^* \rightarrow SiH* + H + H_2 \text{ (threshold at 8.4 eV [15])} \quad (12)$$
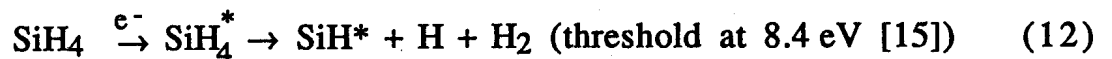
This reaction is a one electron process and depends on the hot electron behaviour (threshold at 8.4 eV). The behaviour of the emission can then be explained in the same terms as for the emission of argon which originates from the ground state excitation in the pure argon plasma. In particular, the rapid decay in the afterglow is a consequence of the decay of T_e.

3.4 Emission from a power-modulated plasma of 4% silane diluted in argon

Fig. 7 shows the time-dependent plasma emission for the two optical emission lines described in sections 3.2 and 3.3 above for a plasma consisting of a 4% mixture of silane in argon.

The Ar* and SiH* emission exhibit behaviour both different from each other and different from their respective pure gas plasmas, namely: the SiH* emission initially increases gradually to its steady-state value (in contrast to the Ar* transient peak), and in the afterglow (Fig. 7 (b)) the Ar* lifetime decays in less than $5\,\mu s$ whereas the SiH* lifetime is prolonged to more than $70\,\mu s$.

The rapid decay of Ar* in the afterglow is a consequence of the quenched metastable density in the silane/argon mixture as shown previously in section 3.1. The only source of Ar* is then excitation from the ground state of the argon, which falls rapidly with T_e.

The source of SiH* cannot be dissociative excitation by electron impact of SiH_4 (equation 12) as in the pure silane case, because the emission behaviour of SiH* is not the same as for Ar*; the source of SiH* emission does not, therefore, originate from the single hot electron excitation process in equation 12. The persistence of the SiH* emission in the afterglow implies that the dominant mechanism of production of this SiH* must originate from a lower energy electron population. This lower energy reaction could be the electronic excitation from the ground state of SiH, which can occur with 3 eV electrons:

$$SiH \xrightarrow{e^-} SiH* \text{ (threshold at 3 eV [15])} \tag{13}$$

For this case of strong dilution of silane in argon, two effects combine to increase the SiH density to the extent that SiH* is predominantly produced from SiH excitation and not directly from

SiH_4 dissociation: firstly, the metastable quenching reactions (reactions (4) to (8)) [24, 25] and secondly, argon dilution reduces the probability that SiH is eliminated by secondary reactions with SiH_4. For these diluted plasmas, the silane is likely to be almost completely depleted. The slow decay of SiH* in the afterglow therefore indicates the slow loss of SiH (by diffusion and by secondary reactions with silane) convoluted with the falling electron density and temperature. The slow rise of SiH* at the onset of the "power on" half-cycle, instead of a peak, would be due to the gradual re-creation of SiH radicals formed predominantly by quenching of argon metastables (as soon as the latter are formed by electron impact on ground state argon atoms) and by direct electron impact dissociation of silane.

4 Conclusions

The time-dependent density of argon metastables has been measured for a pure argon plasma and an argon plasma containing 4% of silane by time-resolved optical absorption spectroscopy. Analysis of the results enables an identification of the destruction mechanisms for these metastable states. The metastable density is strongly reduced by molecular quenching on silane, which also causes silane dissociation.

Complementary plasma emission measurements also show the formation mechanisms of excited species. The importance of electronic excitation from metastables during the afterglow has been demonstrated for pure argon plasmas. The persistence of SiH* emission in silane/argon mixtures is the consequence of an increase

in the dissociation rate of the silane by metastable and electronic collisions, which implies that SiH_4 is likely to be almost completely depleted.

These experiments together show the important role played by argon metastables in silane plasmas diluted with argon. Quenching of the metastables on silane increases the silane dissociation rate. Argon, therefore, is not simply a buffer gas which reduces the secondary reaction probability between radicals and molecules of silane, but plays an active part in the dissociation of silane in argon-diluted silane plasmas.

Acknowledgments

References

[1] Kroll U, Finger F,.Dutta J, Keppner H, Shah A, Howling A A, Dorier J-L and Hollenstein Ch 1992 *Mat. Res. Soc. Proc.* **258** 135

[2] Hollenstein Ch, Kroll U, Howling A A, Dutta J, Dorier J-L, Meier J, Tscharner R and Shah A 1992 *Proc.11th European PV Solar Energy Conf. (Montreux)* p 132

[3] Knights J C, Lujian R A, Rosenblum M P, Street R A, Bieglesen D K, and Reimer J A 1981 *Appl. Phys. Lett.* **38** 331

[4] Matsuda A, Mashima S, Hasezaki K, Suzuki A, Yamasaki S and McElheny P J 1991 *Appl. Phys. Lett.* **58** 2494

[5] Vanier P E, Kampas F J, Corderman R R and Rajeswaran G 1984 *J. Appl. Phys.* **56** 1812

[6] Delcroix J-L, Ferreira C M and Ricard A 1975 *Atomes et molécules métastables dans les gaz ionisés.* Edition du C.N.R.S., Paris, France

[7] Ichikawa Y and Teii S 1980 *J. Phys. D: Appl. Phys.* **13** 1243

[8] Ferreira C M, Loureiro J and Riccard A 1985 *J. Appl. Phys.* **57** 82

[9] Kubota T, Morisaki Y, Ohsawa A and Ohuchi M 1992 *J. Phys. D: Appl. Phys.* **25** 613

[10] Scheller G R, Gottscho R A, Graves D B and Intrator T 1988 *J. Appl. Phys.* **64** 598

[11] Gerasimov G N and Ya Petrov S 1977 *Opt. Spectrosc.* (USSR) **43** 7

[12] Scheller G R, Gottscho R A, Graves D B and Intrator T 1988 *J. Appl. Phys.* **64** 4384

[13] Watanabe Y, Shiratani M, Kubo Y, Ogawa I and Ogi S 1988 *Appl. Phys. Lett.* **53** 1263

[14] Howling A A, Hollenstein Ch and Paris P-J 1991 *Appl. Phys. Lett.* **59** 1409

[15] Cicala G, Losurdo M, Capezzuto P and Bruno G 1992 *Plasma Sources Sci. Technol.* 1 1

[16] Booth J P and Sadeghi N 1991 *J. Appl. Phys.* 70 611

[17] Hansen S G, Luckman G and Colson S D 1988 *Appl. Phys. Lett.* 53 1588

[18] Howling A A, Dorier J-L, Hollenstein Ch, Kroll U and Finger F 1992 *J. Vac. Sci. Technol.* A 10 1080

[19] Jolly J and Touzeau M 1975 *J. Quant. Spectrosc. Radiat. ransfer.* 15 863

[20] Overzet L J and Hopkins M B 1993 *Appl. Phys. Lett.* 63 2484

[21] Theuws P 1981 *Thesis: Molecular beam sampling of a Hollow cathode arc* Eindhoven

[22] Chang J S,chikawa Y I, Hobson R M, Matsumura S and Teii S 1992 *J. Appl. Phys.* 72 2632

[23] Kushner M J 1988 *J. Appl. Phys.* 63 2532

[24] Robertson R and Gallagher A 1986 *J. Appl. Phys.* 59 3402

[25] Mataras D, Cavadias S and Rapakoulias D 1989 *J. Appl. Phys.* 66 1 1 9

[26] Chang R S F and Setser D W 1978 *J. Chem. Phys.* 69 3885

[27] YoshidaT, Ichakawa Y and Sakai H 1989 *Proc. 9th. European PV Solar Energy Conf. (Freiburg)* p 1006

[28] Hopkins M B and Graham W G 1991 *J. Appl. Phys.* 69 3461

[29] Kampas F J and Griffith R W 1981 *J. Appl. Phys.* 52 1285

[30] Perrin J and Schmitt J P M 1982 *Chem. Phys.* 67 167

Figure Captions

Figure 1. Experimental arrangement with a schematic diagram of the rf power modulation circuit and the time-resolved optical spectroscopy.

Figure 2. A partial schematic energy diagram of the argon atom.

Figure 3. Evolution of the argon metastable density (level $1s_5$) during a power modulation period for an argon plasma (●) and for a 4% silane-in-argon plasma (□).

Figure 4. Temporal evolution of the argon emission ($\lambda = 696.54$ nm) for a pure argon plasma modulated at 1 kHz. (a) shows the whole modulation period and (b) shows the detail of the intensity decay in the first 70 μs of the afterglow.
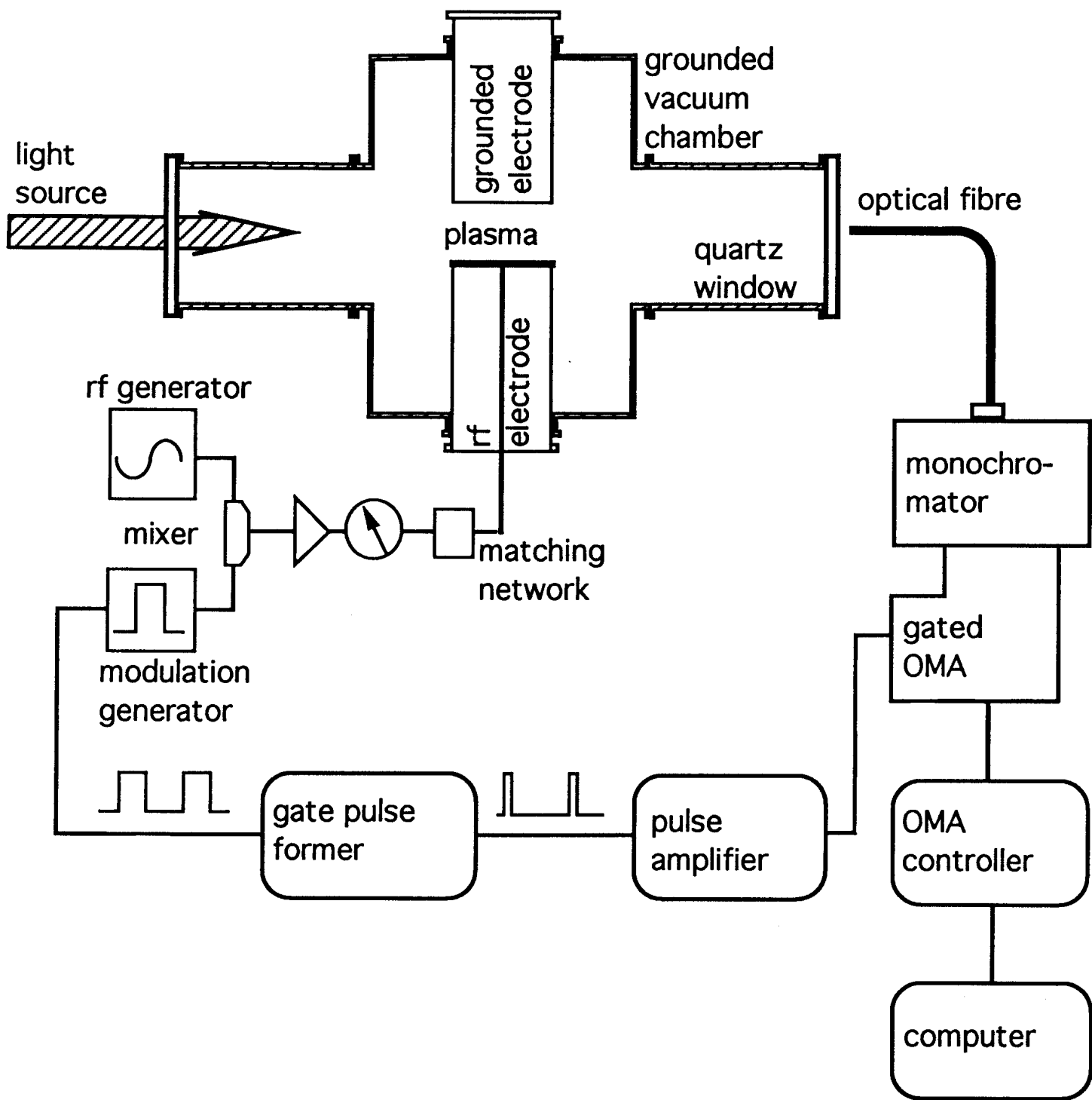
Figure 5. Dependency on T_e of the ratio of the electronic excitation of argon from the ground state ($1s_0$) with the electronic excitation from the metastable levels ($1s_3, 1s_5$) to the $2p_2$ level for an argon plasma with $3.5 \ 10^{15}$ cm^{-3} ground state atoms and $1 \ 10^{11}$ cm^{-3} metastable atoms.

Figure 6. Temporal evolution of the SiH emission ($\lambda = 414.23$ nm) for a pure silane plasma modulated at 1 kHz. (a) shows the whole modulation period and (b) shows the detail of the intensity decay in the first 20 μs of the afterglow.

Figure 7. Temporal evolution of the argon (λ = 696,54 nm) ($\square$) and the SiH (λ = 414.23 nm) ($\bullet$) emission for an argon plasma with 4% silane modulated at 1 kHz. (a) shows the whole modulation period and (b) shows the detail of the intensity decay in the first 70 μs of the afterglow.

light source

grounded vacuum chamber

grounded electrode

plasma

rf electrode

quartz window

optical fibre

rf generator

mixer

modulation generator

matching network

monochro-mator

gated OMA

gate pulse former

pulse amplifier

OMA controller

computer

Figure 1 of 7
L Sansonnens et al
"Role of met..."
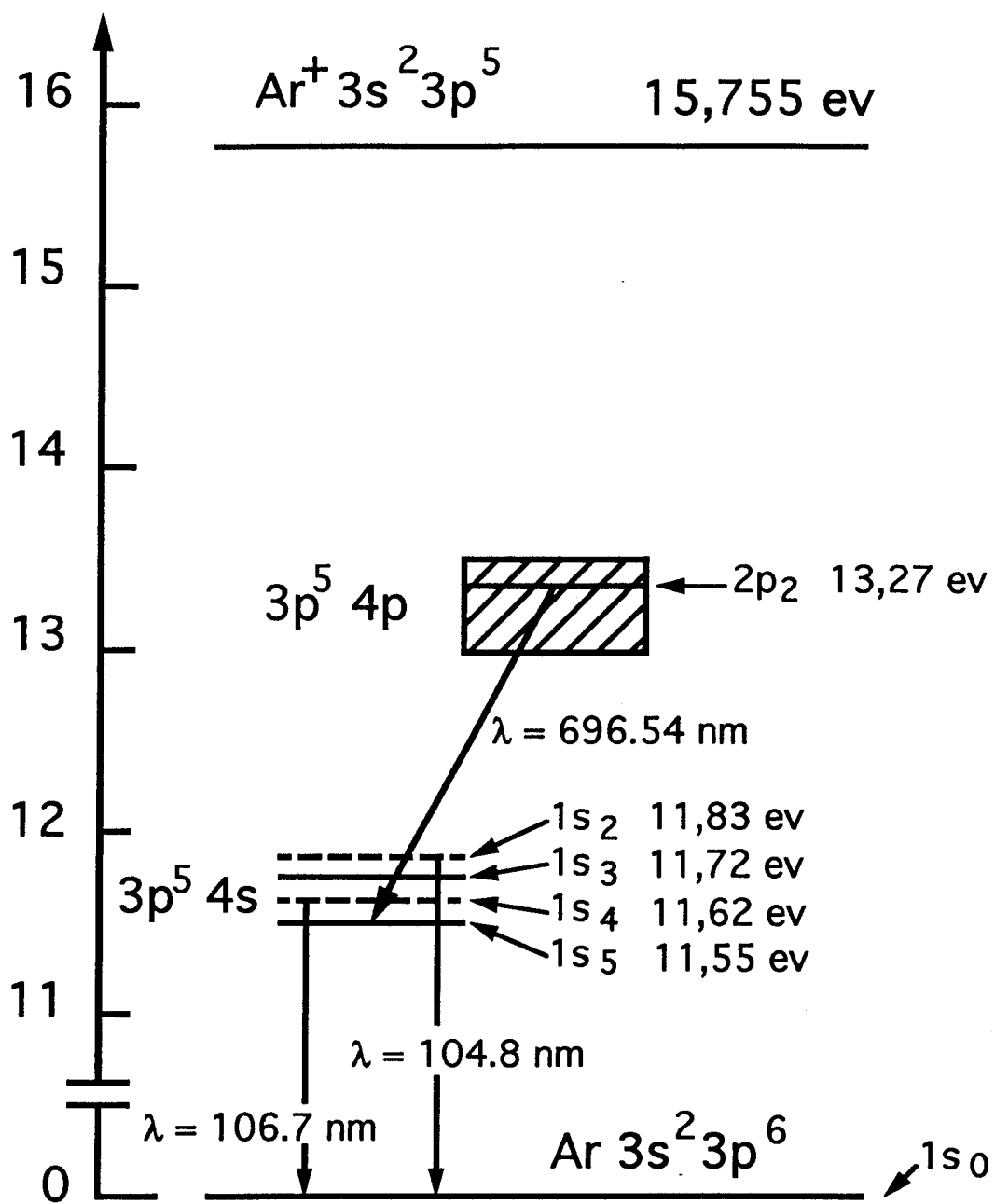
Figure 2 of 7
L Sansonnens et al
"Role of met..."
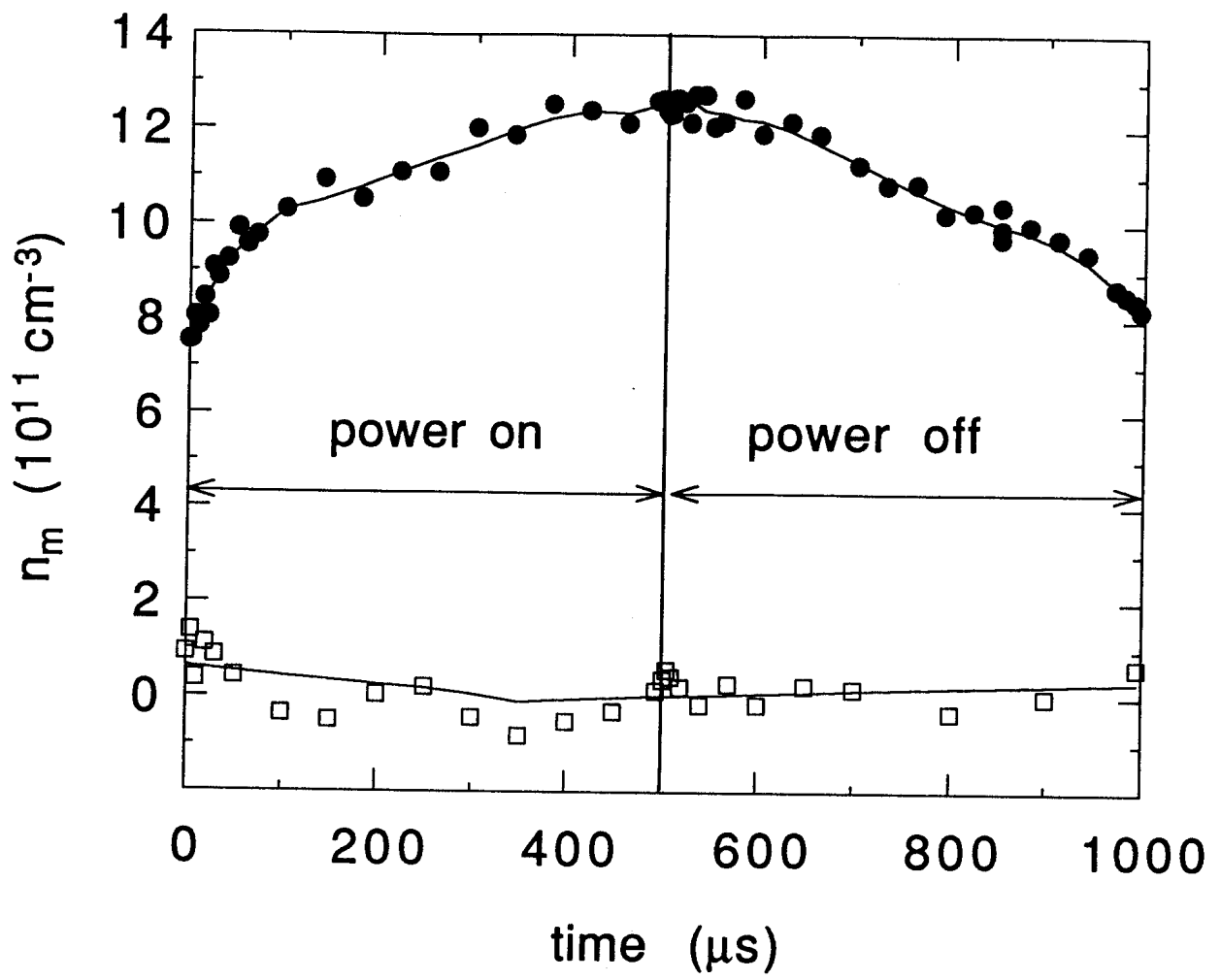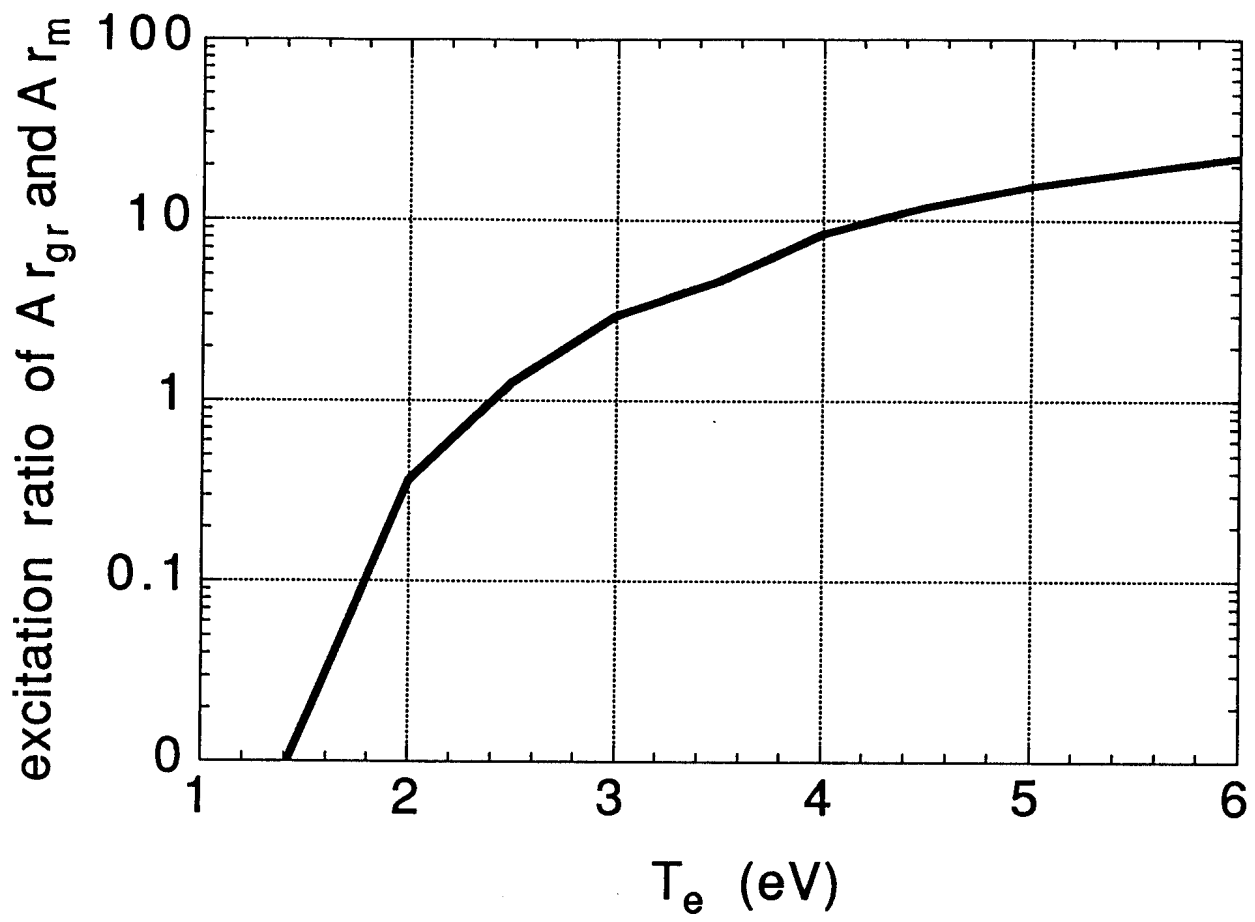
Figure 3 of 7
L Sansonnens et al
"Role of met..."
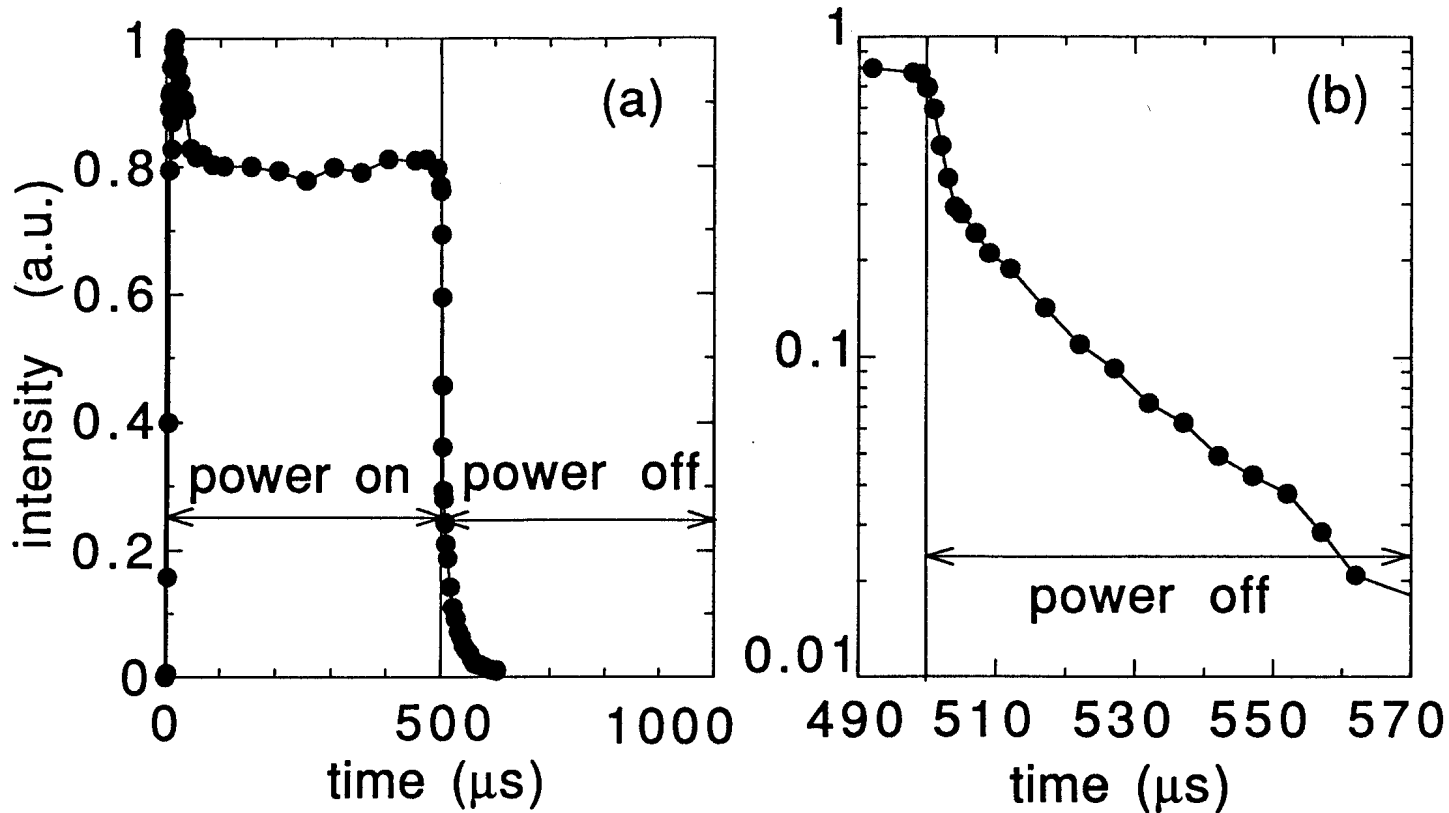
Figure 4 of 7
L Sansonnens et al
"Role of met..."

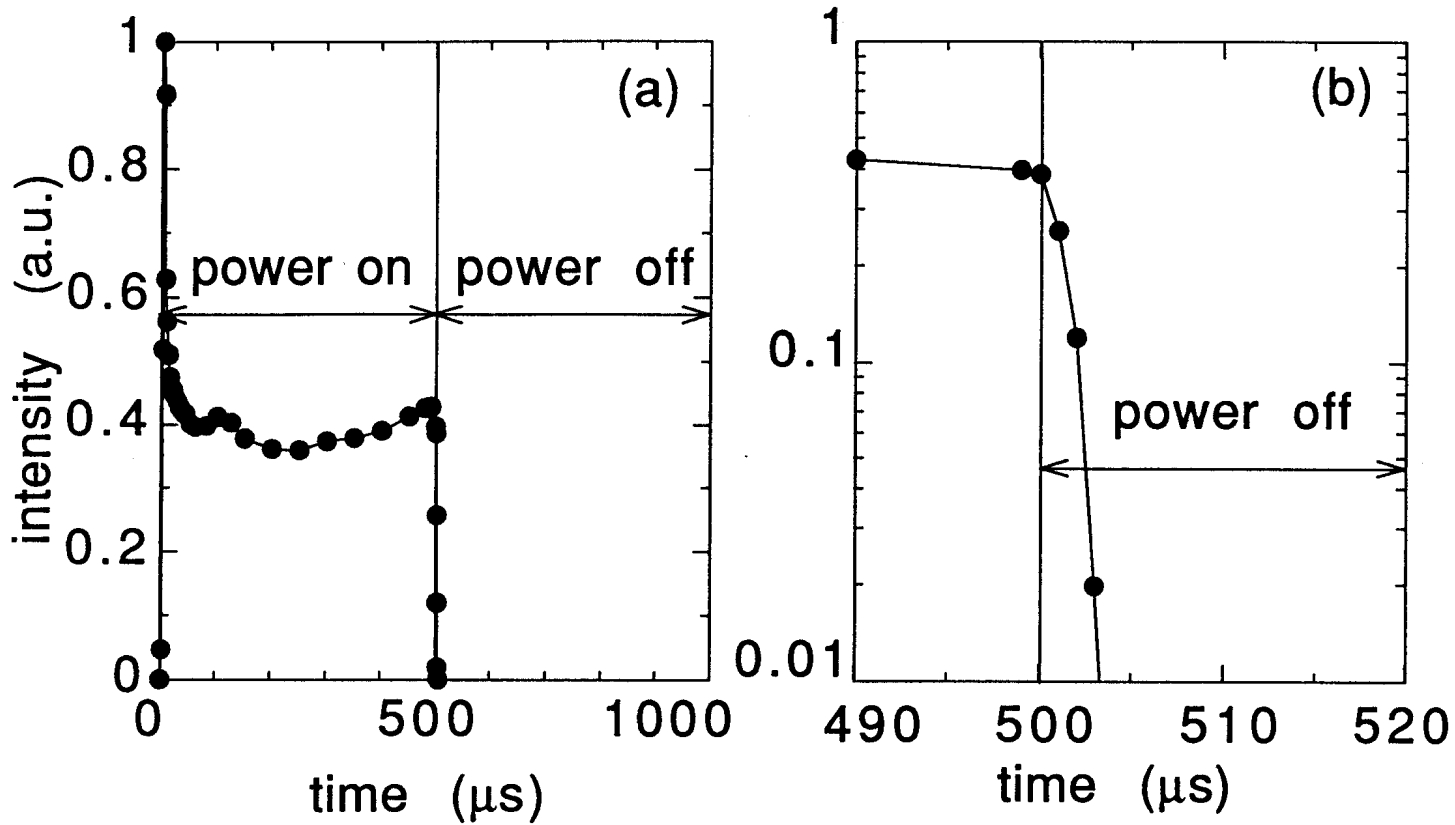Figure 5 of 7
L Sansonnens et al
"Role of met..."

Figure 6 of 7
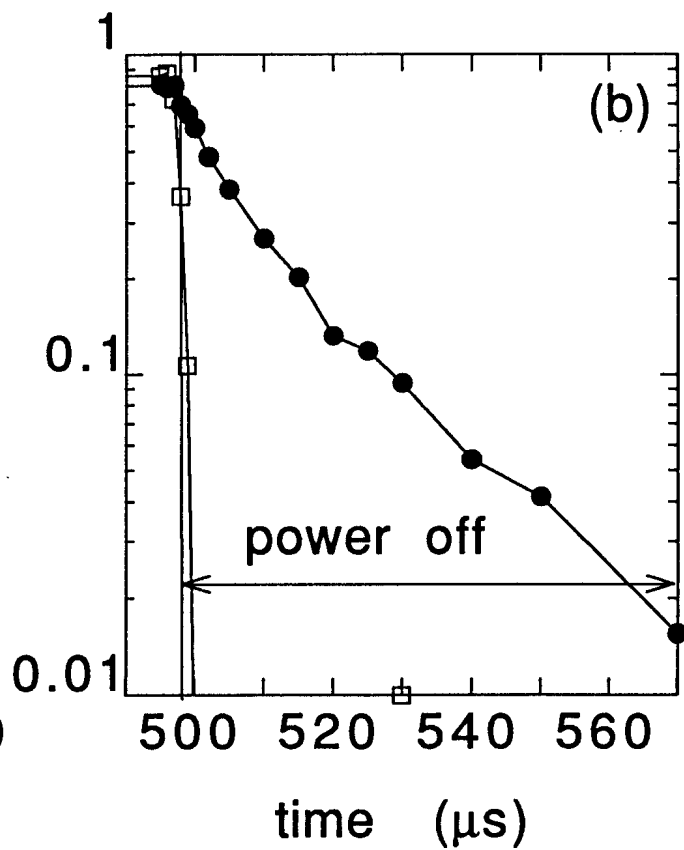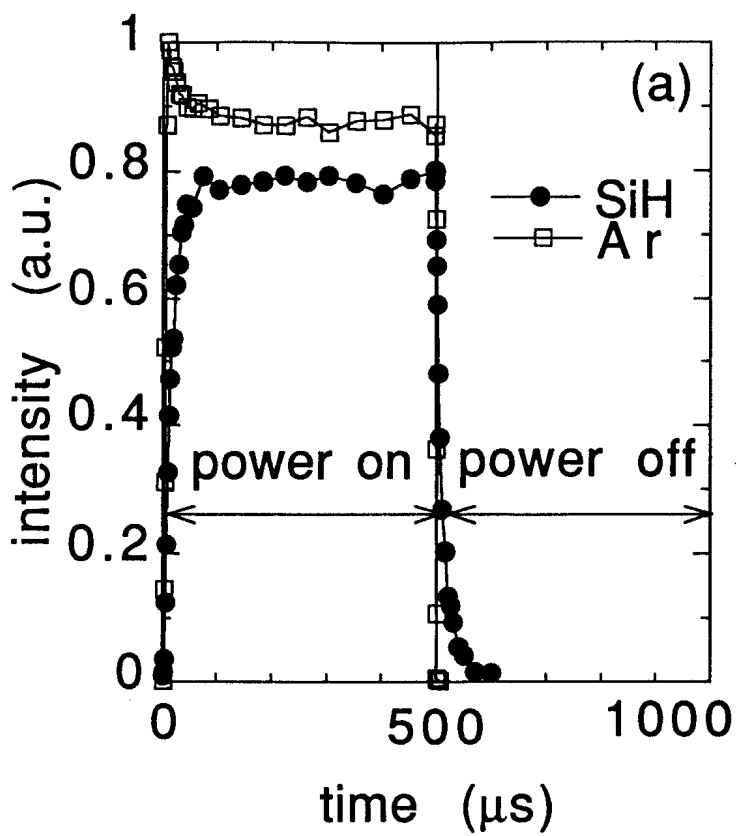L Sansonnens et al
"Role of met..."

Figure 7 of 7
L Sansonnens et al
"Role of met..."